Influence of π-Ligand Substitutions on the Regiospecificity and Stereospecificity in Isospecific Zirconocenes for Propene Polymerization. A Molecular Mechanics Analysis

Massimiliano Toto,[†] Luigi Cavallo,[†] Paolo Corradini,[†] Gilberto Moscardi,[‡] Luigi Resconi,[‡] and Gaetano Guerra*[,§]

Dipartimento di Chimica, Università di Napoli, Via Mezzocannone 4, I-80134, Napoli, Italy, Montell Polyolefins, G. Natta Research Center, P. le G.Donegani 12, I-44100, Ferrara, Italy, and Dipartimento di Chimica, Università di Salerno, I-84081 Baronissi, Salerno, Italy

Received February 17, 1998

ABSTRACT: A possible rationalization of the dependence of regiospecificity of propene polymerization for catalytic systems based on C_2-symmetric *ansa*-zirconocenes (and hafnocenes) on the π-ligand alkyl substitutions is presented. With this aim, models of preinsertion intermediates and transition states for primary and secondary monomer insertion reactions are compared through molecular mechanics analyses. The nonbonded energy contributions to the regioselectivity, as well as the enantioselectivities of regioregular and regioirregular insertion steps have been investigated. Nonbonded energy interactions are able to account for the increases of regiospecificity experimentally observed for zirconocene-based catalytic systems when the π-ligands are alkyl substituted in position 2 or 3 as well as the decrease of regiospecificity observed when the π-ligands are dimethyl substituted in positions 4 and 7.

1. Introduction

Homogeneous catalytic systems composed of chiral C_2-symmetric group 4 metallocenes[1] and methylaluminoxane produce isotactic polypropylene (iPP) by enantiomorphic site control.[2] The mechanism of isospecific propene polymerization with these metallocene catalysts has been rationalized by some of us[3] and others[4] by molecular mechanics analyses on monometallic model complexes.

Contrary to iPP samples produced by catalytic systems based on titanocenes, which are always highly regioregular,[2,5] the iPP samples from catalytic systems based on zirconocenes and hafnocenes contain isolated secondary propene units (2,1 insertions, usually 0−2%) and isolated 3,1 propene units (arising from the unimolecular isomerization of 2,1 units, 0−5%) in the isotactic sequences of primary propene insertions.[6] Typical C_2-symmetric ligands suitable for zirconocene catalyst precursors are sketched in Chart 1.

It has been well established that, contrary to the use of the C_2-symmetric isospecific catalysts, syndiospecific[7] and aspecific[8] zirconocenes are highly regiospecific. Molecular mechanics calculations clearly indicated that intermediates that are energetically suitable for the secondary and primary insertions, for isospecific or syndiospecific complexes, coordinate monomer enantiofaces of opposite or same chirality, respectively.[3e,9] This difference is able to account for the lower regiospecificity of the isospecific catalytic complexes, with the assumption that the energy barrier for the rotation of the coordinated monomer between the orientations suitable for the primary and secondary insertions is lower than the activation energy for the secondary monomer insertion.[9]

In fact, in that framework, for the isospecific models, the low-energy secondary insertion pathway (occurring for the propene enantioface unsuitable for the primary insertion) is only competing with the dissociation of the coordinated monomer and with the high-energy primary insertion (determining the stereoirregularities). On the contrary, for the syndiospecific as well as for the aspecific models, the low-energy secondary insertion pathway (occurring for the propene enantiofaces suitable for the primary insertion) is competing with the very low-energy primary insertion pathway.

Chart 1

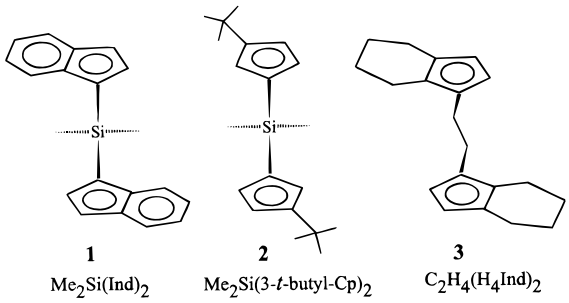

For isospecific *ansa*-zirconocene catalysts, regioirregularities can also be reduced when the C_2-symmetric ligand contains, in addition to the enantioselectivity-determining substituent in the 4 (β) positions, an alkyl group in the 2 (α) positions.[10] Some data relative to the regiospecificity of catalytic systems based on **1** and **2**, after methyl substitution of position 2, are reported in Table 1. Moreover, for catalytic systems based on C_2-symmetric, bridged bis(1-indenyl) ligands, regioirregularities are substantially absent when *tert*-butyl groups are substituted in position 3 (β').[11a,b] On the other hand, regioirregularities are increased when the indenyl ligands are substituted in both positions 4 and 7.[12] In particular, a remarkable amount of regioirregularities close to 20% is observed for the case of the catalytic system based on *rac*-ethylene(4,7-dimethyltetrahydro-1-indenyl)$_2$ZrCl$_2$.[6l,13] Some data relative to the regiospecificity of catalytic systems based on **1** and

[†] Università di Napoli.
[‡] G. Natta Research Center.
[§] Università di Salerno.

S0024-9297(98)00238-1 CCC: $15.00
Published on Web 05/12/1998

Table 1. Propylene Polymerizations with Racemic Zirconocene/MAO Catalysts

	zirconocene ligand	% regioinversions	ref
1	$Me_2Si(Ind)_2$	0.4_8[a]	12
	$Me_2Si(2\text{-}MeInd)_2$	0.3_3[a]	9
	$Me_2Si(4,7\text{-}Me_2Ind)_2$	1.8_4[a]	9
2	$Me_2Si(3\text{-}t\text{-}BuCp)_2$	1.5[b]	10a
	$Me_2Si(2\text{-}Me\text{-}4\text{-}t\text{-}BuCp)_2$	0.4	10a
3	$C_2H_4(H_4Ind)_2$	0.9_7[a]	13
	$C_2H_4(4,7\text{-}Me_2H_4Ind)_2$	18.9	13

[a] Polymerization conditions: 1 L stainless-steel autoclave, propene 0.4 L, 50 °C, zirconocene/MAO aged 10 min. [b] Polymerization conditions: propene 2 bar, 50 °C, ziroconocene/Al = 1/300.

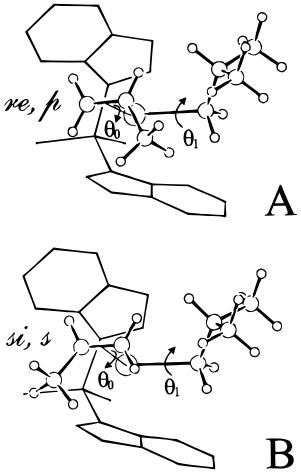

Figure 1. One of the model catalytic complexes used in our computations, which comprises the (*R,R*)-*rac*-$Me_2Si(Ind)_2$ ligand, a propene molecule (shown for the *re* and *si* coordination in parts A and B, respectively), and an isobutyl group simulating a polypropene growing chain. The dihedral angle θ_0 associated with rotations of the olefin around the axis connecting the metal to the center of the double bond, and the internal rotation angle θ_1 associated with rotations around the bond between the metal atom and the first carbon atom of the growing chain are indicated. The conformation depicted in A corresponds to $\theta_0 = 0°$ and $\theta_1 = -60°$, which is suitable for the monomer primary (*p*) insertion. The conformation depicted in B corresponds to $\theta_0 = 180°$ and $\theta_1 = -60°$, which is suitable for the monomer secondary (*s*) insertion.

3, after dimethyl substitutions of the positions 4 and 7 of both π-ligands, are also reported in Table 1.

In the present molecular mechanics study, catalytic intermediates and possible transition states for the primary and secondary monomer insertion reactions are compared, in order to evaluate the nonbonded energy contributions to regioselectivity for different C_2-symmetric *ansa*-zirconocene model complexes. The aim is a possible rationalization of the dependence of regiospecificity of catalytic systems based on C_2-symmetric *ansa*-zirconocenes (and hafnocenes) on the π-ligand alkyl substitutions.

2. Models and Computational Details

2.1. Models. As in previous papers,[3] the basic models of the alkene-bound intermediates here considered are metal complexes containing three ligands, that is a π-coordinated propene molecule, a σ-coordinated isobutyl group (simulating a primary growing chain), and a stereorigid π-coordinated ligand.

We recall the definitions of the most important internal coordinates that have been varied (see Figure 1A): the dihedral angle θ_0 associated with rotations of the olefin around the axis connecting the metal to the center of the double bond and the internal rotation angle θ_1 associated with rotations around the bond between the metal atom and the first carbon atom of the growing chain. At θ_0 near 0° the olefin is oriented in a way suitable for primary insertion, while θ_0 near 180° corresponds to an orientation suitable for secondary insertion. θ_1 near 0° corresponds to the conformation having the first C−C bond of the growing chain eclipsed with respect to the axis connecting the metal atom to the center of the double bond of the olefin.

A prochiral olefin such as propene may give rise to nonsuperposable coordinations, which can be labeled with the notation *re* and *si*.[14] The coordination of the C_2-symmetric ligand is chiral, and can be labeled with the notation (*R*) or (*S*) according to the rules of Cahn−Ingold−Prelog[15] extended to chiral metallocenes as outlined by Schlögl.[16] The symbols (*R*) and (*S*) indicate the absolute configuration of the bridgehead carbon atom of the indenyl groups, for the C_2-symmetric ligand. Without loss of generality, all the reported calculations refer to the (*R,R*) coordination of the C_2-symmetric ligand. Moreover, as for the coordination of the ethylene(4,7-dimethyltetrahydro-1-indenyl)$_2$ ligand, which also presents a chirality at the C atoms in positions 4,7 and 4′,7′, we considered the ligand with *R* and *S* chirality at the C atoms in positions 4,4′ and 7,7′, respectively. In fact, this is the diastereoisomer for which experimental data are available. It is worth noting that, with these chiralities at the 4,4′ and 7,7′ C atoms, the methyl substituents point toward the Zr center.

We also recall that, in the framework of our analysis, the conformations of alkene-bound intermediates are considered sufficiently close to the transition state and considered as suitable conformers of *preinsertion intermediates*, only if the insertion can occur through a process of "least nuclear motion".[17] This corresponds to geometries of the alkene-bound intermediates for which[17a,d,e] (i) the double bond of the olefin is nearly parallel to the bond between the metal atom and the growing chain ($\theta_0 \approx 0°$ or $\theta_0 \approx 180°$) and (ii) the first C−C bond of the chain is nearly perpendicular to the plane defined by the double bond of the monomer and by the metal atom ($|\theta_1| \approx 60-90°$ rather than $\theta_1 \approx 180°$). Let us recall that θ_1 values away from 180° and near ±60° are also suited for the formation of an α-agostic bond, which has been shown to stabilize the transition state for the insertion step in some scandium- and zirconium-based catalysts.[18]

We assume that the energy differences between suitable preinsertion intermediates are close to those present in the corresponding transition states for the insertion reaction.

The molecular mechanics calculations have been performed also on *pseudotransition states*, for which the geometry of the olefin and of the first carbon atom of the growing chain has been set equal to that determined by Ziegler for the insertion reaction $[Cp_2ZrCH_3]^+ + CH_2{=}CH_2 \Rightarrow [Cp_2ZrCH_2CH_2CH_3]^+$.[19]

As a final remark, alkene-bound intermediates for which the methyl group of the propene and the second carbon atom (and its substituents) of the growing chain are on the same side with respect to the plane defined by the Mt−C bonds ($\theta_1 \approx +60°$ and −60° for the *re*- and *si*-coordinated monomer, respectively) are assumed to be unsuitable for the successive monomer insertion. In fact, insertion paths starting from these intermediates

involve large nonbonded interactions.[17f,g,20] To further investigate this aspect, we also explored the possibility that in the pseudotransition states the methyl group of the propene and the growing chain are on the same side with respect to the plane defined by the four-atom transition state. For all the considered systems, these situations are of higher energy (at least 3 kcal/mol) with respect to the situations in which the methyl group of the propene and the growing chain are on opposite sides.

2.2. Calculation Method. The computational details can be found elsewhere,[9] and for the sake of simplicity are not reported here. We only recall that although the numerical values of the energy differences depend also on the exact geometry and on the energy parameters adopted in the calculations, no reasonable adjustment of these parameters seems to be able to modify our conclusions. The results presented in this paper are obtained within the scheme developed by Bosnich for bent metallocenes.[21] The approach used by Bosnich is a development of the CHARMM force field of Karplus,[22] to include group 4 metallocenes. With respect to the scheme developed by Bosnich, we only assumed that the bending force constant relative to the angle formed by the Zr atom, the center of the cyclopentadienyl ring, and the C atoms of the ring itself is equal to the analogous bending force constant involving the Ti atom. Our feeling is that the original constant proposed by Bosnich is adequate to describe also hindered dichlorides but is somewhat too stiff to properly describe the tendency of hindered systems to adopt η^3 coordination of the cyclopentadienyl rings. In particular, the pattern of short, medium, and long Zr−C distances of 2.44, 2.56, and 2.72 Å, experimentally observed for $Me_2Si(Flu)_2ZrCl_2$,[23] is better reproduced by using the softer bending force constant proposed for Ti (2.48, 2.56, and 2.71 Å) than by using the harder bending force constant proposed for Zr (2.50, 2.56, and 2.66 Å). This feature is of great relevance when the more bulkier olefin and growing chain replace the chlorine atoms. On the other hand, for the less hindered systems, nearly identical results are obtained by using the bending constant proposed for Ti or for Zr.

To model the olefin coordination, we adopted the scheme proposed by Bosnich to model the coordination of a cyclopentadienyl ring to the metal atom. The parameters involving the center of the olefin have been assumed to be equal to the analogous ones involving the center of the cyclopentadienyl ring. The equilibrium distance between the Zr atom and the C atoms of the olefin, as discussed in detail in ref 3e, has been set to 2.5 Å and, as a consequence, the equilibrium distance between the Zr atom and the center of the olefin double bond has been assumed to be 2.39 Å.

As for the molecular mechanics analysis of the pseudotransition states, the geometry of the olefin and of the first carbon atom of the growing chain has been set equal to that determined by Ziegler for the insertion reaction $[Cp_2ZrCH_3]^+ + CH_2{=}CH_2 \Rightarrow [Cp_2ZrCH_2CH_2CH_3]^+$.[19] In particular, the distance of the Zr−C (chain) bond that is going to be broken, the distance Zr−C (olefin) and C(olefin)−C(chain) of the bonds that are going to be formed, and the C−C olefin bond distance have been set equal to 2.24, 2.39, 2.38, and 1.38 Å, respectively. The bond distances and the bending angles of the atoms involved in the breaking and forming of bonds are not varied, whereas torsional angles involving such atoms have been constrained to be ±15° from the values determined by Ziegler.

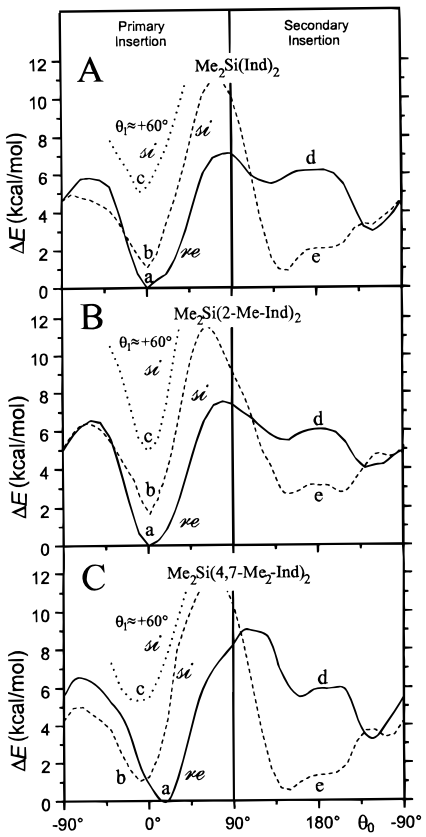

Figure 2. Optimized energies as a function of θ_0 for the model complex with the C_2-symmetric (*R*,*R*)-*rac*-$Me_2Si(Ind)_2$ ligand presenting indenyl groups: (A) unsubstituted; (B) 2-methyl substituted; (C) 4,7-dimethyl substituted. The full and dashed lines refer to *re*- and *si*-coordinated propene, respectively, and correspond to a θ_1 value close to −60°. The dotted lines are a part of the optimized energy curve obtained by imposing, for the *si*-coordinated monomer, that the methyl group of the propene and the second carbon atom (and its substituents) of the growing chain are on opposite sides with respect to the plane defined by the Zr−C bonds (i.e., imposing $\theta_1 \approx +60°$). Models corresponding to minimum energy situations with $\theta_0 \approx 0°$ and with $\theta_0 \approx 180°$ (intermediates for primary and secondary insertion, respectively), labeled a and e in A, B, and C, are sketched in Figures 1, 3, and 4 (parts A and B), respectively.

3. Results and Discussion

3.1. Ligand Substitutions in Position 2 and in Positions 4 and 7. Figure 2A plots as a function of θ_0 the optimized energies (reprinted from ref 9) for the model complex with ligand **1** with (*R*,*R*) chirality of coordination. The absolute minimum energy situation is labeled a in Figure 2A and corresponds to the *re* monomer coordination with a value of $\theta_0 \approx 0°$. The corresponding model is sketched in Figure 1A. This model minimizes the interactions between the growing chain (at $\theta_1 \approx -60°$) and the methyl of the *re*-coordinated propene monomer. Therefore, it is assumed to be a preinsertion intermediate suitable for the *re* monomer primary insertion.

A slightly higher energy is calculated for the minimum energy geometry labeled as b in Figure 2A, which corresponds to the *si* monomer coordination with values of $\theta_0 \approx 0°$ and $\theta_1 \approx -60°$. However, this situation is considered unsuitable for the successive monomer in-

Table 2. Calculated Enantioselectivities for Primary ($\Delta E_{enant,p}$) and Secondary ($\Delta E_{enant,s}$) Insertions and Nonbonded Energy Contributions to the Regiospecificity (ΔE_{regio}), for Preinsertion Intermediates[a]

	(*R*,*R*)-coordinated ligand	$\Delta E_{enant,p}$	$\Delta E^*_{enant,p}$	favored enantioface	$\Delta E_{enant,s}$	favored enantioface	ΔE_{regio}	ΔE^*_{regio}
1	$Me_2Si(ind)_2$	4.9	3.0	*re*	4.0	*si*	2.1	2.4
	$Me_2Si(2\text{-}MeInd)_2$	4.8	3.2	*re*	2.6	*si*	3.1	3.1
	$Me_2Si(4,7\text{-}Me_2Ind)_2$	5.2	3.1	*re*	4.2	*si*	1.4	1.5
	$Me_2Si(3\text{-}MeInd)_2$	0.1	0.3	*re*	2.8	*si*	1.7	1.9
	$Me_2Si(3\text{-}t\text{-}BuInd)_2$	4.0	2.4	*si*	0.8	*si*	4.2	4.0
2	$Me_2Si(3\text{-}t\text{-}BuCp)_2$	6.4	5.0	*re*	3.7	*si*	0.2	0.6
	$Me_2Si(2\text{-}Me\text{-}4\text{-}t\text{-}BuCp)_2$	8.9	5.9	*re*	2.6	*si*	1.7	1.5
3	$C_2H_4(H_4Ind)_2$	5.7	4.7	*re*	5.3	*si*	2.0	3.9
	$C_2H_4(4,7\text{-}Me_2H_4Ind)_2$	6.1	10.1	*re*	5.6	*si*	−1.0	1.3

[a] The starred ΔE values have been calculated for pseudo-transition states.

sertion. In fact, the methyl group of the propene and the second carbon atom (and its substituents) of the growing chain are on the same side with respect to the plane defined by the Zr−C bonds. The dotted line shown in Figure 2A refers to the optimized energy curve obtained by imposing $\theta_1 \approx +60°$ for the *si* monomer coordination. The corresponding energy minimum is labeled as c. It is nearly 5 kcal/mol higher than the absolute minimum, and it is assumed to be a preinsertion intermediate suitable for the *si* primary insertion. The optimized energy corresponding to $\theta_0 = 180°$ for the *si* monomer coordination, labeled as e in Figure 2A, is higher by nearly 2 kcal/mol with respect to the absolute minimum. The corresponding model sketched in Figure 1B is considered suitable for *si* monomer secondary insertion. As already discussed in detail for the isospecific model sites including the ethylenebis(1-indenyl) and ethylenebis(4,5,6,7-tetrahydro-1-indenyl) ligands,[3e] the situation corresponding to $\theta_0 = 180°$ for the *re* monomer coordination, labeled as d in Figure 2A, is of much higher energy.

In our framework, the energy differences $E_c - E_a$ and $E_d - E_e$ give approximations of the enantioselectivities of primary ($\Delta E_{enant,p}$) and of secondary ($\Delta E_{enant,s}$) insertion steps, respectively. Moreover, the energy difference $E_e - E_a \approx 2$ kcal/mol gives an approximation of the nonbonded energy contribution to the regiospecificity (ΔE_{regio}).[24]

In summary, for the model complex based on ligand **1**, there is a substantial enantioselectivity for primary (largely prevailing) as well as for secondary monomer insertion. The enantioselectivity is due to nonbonded energy interactions of the methyl group of the chirally coordinated monomer with the chirally oriented growing chain, for the primary insertion, and with the chirally coordinated π-ligand, for the secondary insertion.[3,9]

Parts B and C of Figure 2 plot as a function of θ_0 the optimized energies for the model complex with an (*R*,*R*)-coordinated ligand **1**, presenting both indenyl groups methyl substituted in position 2 or dimethyl substituted in positions 4 and 7, respectively. The energy curves of Figure 2B,C are similar to those of Figure 2A. There is only an increase of the nonbonded energy contribution to the regiospecificity ($\Delta E_{regio} = E_e - E_a$) for the 2-methyl-substituted model and a decrease for the 4,7-substituted model.

Molecular mechanics calculations have been performed also on pseudotransition states, constructed as described in the previous section, corresponding to the preinsertion intermediates labeled as a, c, and e in Figure 2. Pseudotransition states presenting the methyl group of the propene and the second carbon atom of the growing chain on the same side with respect to the plane defined by the Zr−C bonds, which correspond to preinsertion intermediates labeled as b in Figure 2, have been also considered. However, for all the considered models, the pseudotransition states corresponding to the preinsertion intermediates labeled as b in Figure 2 present energies higher by at least 3 kcal/mol with respect to those corresponding to the preinsertion intermediates labeled as c in Figure 2. This supports the previous assumption, done also in previous papers,[3] that $\Delta E_{enant,p} = E_c - E_a$ rather than $E_b - E_a$.

The enantioselectivity for the primary insertion and the nonbonded energy contribution to the regiospecificity, evaluated for pseudotransition states ($\Delta E^*_{enant,p}$ and ΔE^*_{regio}, respectively) are compared to those evaluated for preinsertion intermediates ($\Delta E_{enant,p}$ and ΔE_{regio}, respectively) in Table 2. It is worth noting that the energy differences evaluated for preinsertion intermediates and for pseudotransition states are qualitatively similar. In particular, also for pseudotransition states the nonbonded energy contribution to the regioselectivity increases after methyl substitution in position 2 and decreases after methyl substitutions in positions 4 and 7.

For the case of ligand **1** methyl substituted in position 2, the models corresponding to the minimum energy preinsertion intermediates suitable for primary and secondary insertions (labeled with a and e in Figure 2B), are sketched in Figure 3A,B, respectively. The corresponding pseudotransition states are sketched in Figure 3C,D, respectively. In the models suitable for secondary insertion, a methyl group of the ligand is at a short distance with respect to the methyl group of propene. In particular, for both models, the distance between the two C atoms of the two methyl groups is close to 3.5 Å. On the contrary, for the case of the models for primary insertion, the distances of the methyl substituents from the methyl group of propene are larger than 5 Å. This accounts for the increase of the calculated ΔE_{regio} and ΔE^*_{regio} values, for the ligand **1** after 2-methyl substitution.

For the case of ligand **1** dimethyl substituted in positions 4 and 7, the models of the minimum energy preinsertion intermediate for the primary insertion (labeled with a in Figure 2C) and of the corresponding pseudotransition state are sketched in Figure 4A,C, respectively. Already, on inspection, it is apparent that in both models a methyl group in position 4 is at a short distance with respect to the methyl group of propene. In particular, the distances between the two C atoms are once again close to 3.5 Å. On the contrary, for the models of the minimum energy preinsertion intermediate for the secondary insertion (labeled with e in Figure 2C) and of the corresponding pseudotransition state,

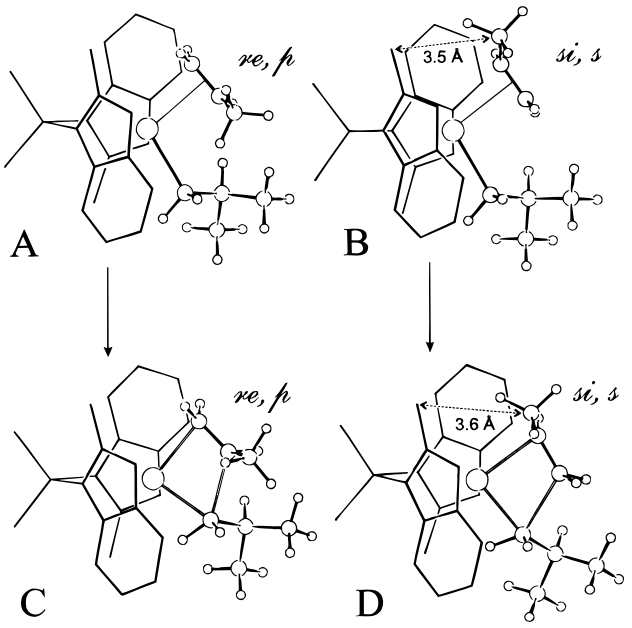

Figure 3. Alkene-bound intermediates (A and B) and pseudotransition states (C and D) for monomer orientations suitable for primary (*p*) and secondary (*s*) insertions into a primary polypropene growing chain, for the case of the (*R*,*R*)-coordinated C_2-symmetric *rac*-$Me_2Si(2\text{-}MeInd)_2$ ligand. (A) and (B) correspond to the situations labeled with letters a and e in Figure 2B and include *re*- and *si*-coordinated propene, respectively. Short nonbonded distances between the methyl group of propene and the methyl substituent of a indenyl group are indicated.

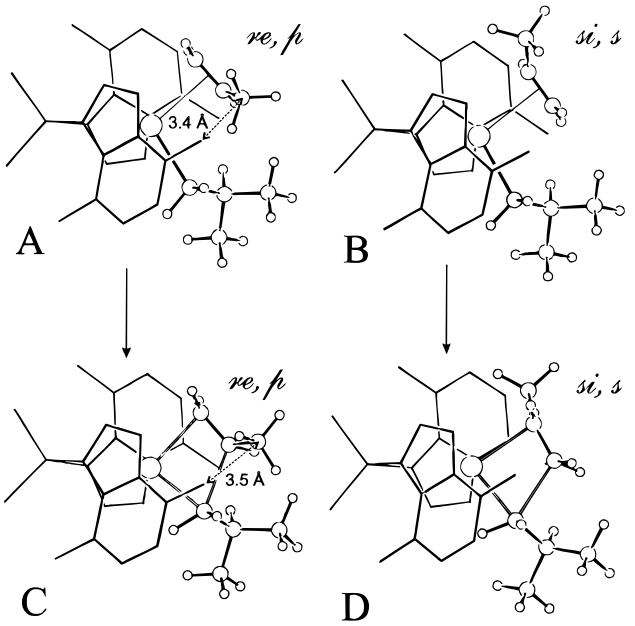

Figure 4. Alkene-bound intermediates (A and B) and pseudotransition states (C and D) for monomer orientations suitable for primary (*p*) and secondary (*s*) insertions into a primary polypropene growing chain, for the case of the (*R*,*R*)-coordinated C_2-symmetric *rac*-$Me_2Si(4,7\text{-}Me_2Ind)_2$ ligand. (A) and (B) correspond to the situations labeled with letters a and e in Figure 2C and include *re*- and *si*-coordinated propene, respectively. Short nonbonded distances between the methyl group of propene and a methyl substituent of the ligand are indicated.

sketched in Figure 4B,D, respectively, the distances of the methyl substituents from the methyl group of propene are larger than 4.5 Å. This accounts for the

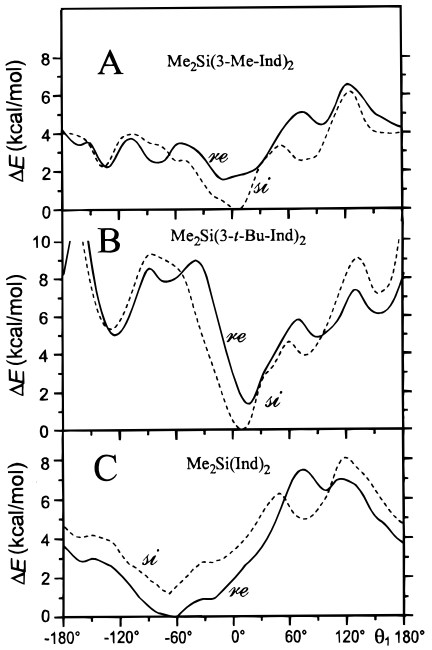

Figure 5. Optimized energies as a function of θ_1 for the model complex with the C_2-symmetric (*R*,*R*)-*rac*-$Me_2Si(Ind)_2$ ligand presenting indenyl groups: (A) 3-methyl substituted; (B) 3-*tert*-butyl substituted; (C) unsubstituted. The full and dashed lines refer to *re*- and *si*-coordinated propene, with $\theta_0 \approx 0°$.

reduction of the calculated ΔE_{regio} and ΔE^*_{regio} values, for the ligand **1** after 4,7-dimethyl substitution.

In summary, the reported calculations relative to the models with ligand **1** (Table 2) are in fair agreement with the observed polymerization behavior of corresponding catalytic systems. In fact, the increase and decrease of the nonbonded energy contribution to the regiospecificity, after 2-methyl and 4,7-dimethyl substitutions (last two columns in Table 2) qualitatively account for the decrease and increase, respectively, of the observed regioirregularities for the corresponding catalytic systems (2nd column in Table 1).

Analogous calculations have been performed for unsubstituted and 2-methyl-substituted ligand **2** as well as for unsubstituted and 4,7-dimethyl-substituted ligand **3**. The corresponding calculated enantioselectivities and nonbonded energy contributions to the regiospecificity are reported in Table 2. Both ΔE_{enant} and ΔE^*_{enant} values in Table 2 indicate that the models with ligands **2** and **3** are highly enantioselective and that, in agreement with the experimental observation, their isospecificity increases for methyl substitutions in position 2.[10a,25]

As for the nonbonded energy contribution to the regiospecificity, it increases by nearly 1 kcal/mol for ligand **2**, after 2-methyl substitution, while it decreases by more than 2 kcal/mol for ligand **3**, after 4,7-dimethyl substitutions (Table 2). These energy differences are produced by nonbonded energy interactions similar to those shown in Figures 3 and 4 and are in good qualitative agreement with the substantial reduction and increase of the percent of regioirregularities for the catalytic system based on ligand **2** after 2-methyl substitution and based on ligand **3** after 4,7-dimethyl substitution, respectively (Table 1).

3.2. Ligand Substitution in Position 3. Parts A and B of Figure 5 plot as a function of θ_1 the optimized energies for the model complex with an (*R*,*R*)-coordinated ligand **1**, presenting both indenyl groups methyl

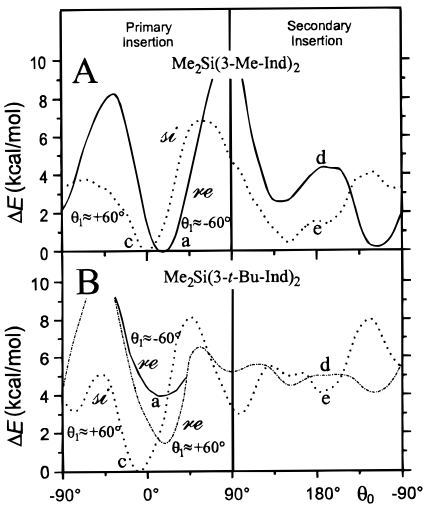

Figure 6. Optimized energies as a function of θ_0 for the model complex with the C_2-symmetric (*R*,*R*)-*rac*-$Me_2Si(Ind)_2$ ligand presenting indenyl groups: (A) 3-methyl substituted; (B) 3-*tert*-butyl substituted. The dotted and the dashed-dotted lines (Figure 6B) refer to *si*- and *re*-coordinated propene, respectively, and correspond to a θ_1 value close to +60°. The full lines refer to *re*-coordinated propene and correspond to $\theta_1 \approx -60°$. Models corresponding to minimum energy situations with $\theta_0 \approx 0°$ and with $\theta_0 \approx 180°$ (intermediates for primary and secondary insertion, respectively), labeled c and e in B, are sketched in Figure 7A,B, respectively.

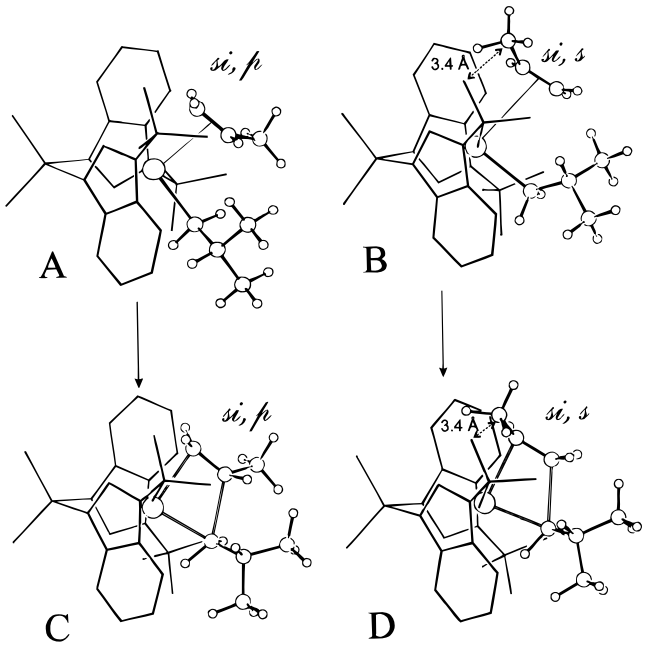

Figure 7. Alkene-bound intermediates (A and B) and pseudotransition states (C and D) for monomer orientations suitable for primary (*p*) and secondary (*s*) insertions into a primary polypropene growing chain, for the case of the (*R*,*R*)-coordinated C_2-symmetric *rac*-$Me_2Si(3\text{-}t\text{-BuInd})_2$ ligand. (A) and (B) correspond to the situations labeled with letters c and e in Figure 6B and include *si*-coordinated propene. Short nonbonded distances between the methyl group of propene and a methyl group of the ligand are indicated.

or *tert*-butyl substituted in position 3, respectively. The energy curves of Figure 5 refer to monomer orientation suitable for primary insertion ($|\theta_0| < 20°$). For these highly hindered model complexes the absolute energy minima are obtained for $\theta_1 \approx 0°$, that is for a growing chain orientation far from the transition states of both primary and secondary insertions. In fact, for this orientation of the growing chain, the second C atom is closer to the monomer than the first C atom of the chain, which is the one supposed to react. It is worth noting that the optimized energy curves present absolute energy minima for situations with $|\theta_1| \approx 60°$ for the less hindered model complexes of Figure 2. This is shown, for instance, for the model complex with unsubstituted ligand **1** in Figure 5C.

Parts A and B of Figure 6 plot as a function of θ_0 the optimized energies for the model complex with an (*R*,*R*)-coordinated ligand **1**, presenting both indenyl groups methyl or *tert*-butyl substituted in position 3, respectively. In order to confine the analysis to suitable preinsertion intermediates, the energy curves of Figure 6 have been obtained under the constraint that $40° < |\theta_1| < 80°$ (as discussed in point ii in section 2.1), ignoring the situations corresponding to the absolute minima for Figure 5A,B ($|\theta_1| < 20°$). The shapes of the energy curves of Figure 6 are substantially different from those of Figure 2A−C. In particular, for situations suitable for primary monomer insertions, the energy *minima labeled c* (for the *si* enantioface and for $\theta_1 \approx +60°$), which *are* much higher than the energy *minima labeled a* (for the *re* enantioface and for $\theta_1 \approx -60°$) for the models of Figure 2, *become* closer to or lower than the energy minima labeled a for the models of Figure 6A,B, that is, after methyl or *tert*-butyl substitution in position 3, respectively.

The enantioselectivities and nonbonded energy contributions to the regiospecificity, evaluated on the basis of the energy curves of Figure 6 are reported in Table 2, together with the values calculated for the corresponding pseudotransition states. The energy curves of Figure 6A and the data of the 2nd and 3rd columns of Table 2 indicate that, in good agreement with the observed behavior of catalytic systems including bridged 3-methylindenyl ligands,[6n,26] the model complex with 3-methyl substitution of ligand **1** is substantially nonenantioselective. This has been already discussed in detail by some of us (although using much more rigid models) in ref 3c.

As generally found for nonenantioselective or poorly enantioselective zirconocene-based catalytic systems,[9] the regiospecificity of this catalytic system is extremely high.[6n] As discussed in ref 9, for aspecific catalytic systems, the regiospecificity is related to the energy differences (electronic and steric) between the activation energies for primary and secondary insertion steps, which are generally large.[27] As a consequence, the calculated nonbonded energy contribution to the regiospecificity, generally small with respect to the electronic contribution, are substantially irrelevant. However, for the sake of comparison with the other model complexes, also the calculated values of ΔE_{regio} and ΔE^*_{regio} are listed in Table 2.

Models corresponding to the minimum energy preinsertion intermediates suitable for the primary and secondary insertions, for the case of 3-*tert*-butyl-substituted ligand **1** (labeled with c and e in Figure 6B), are sketched in Figure 7A,B, respectively. The corresponding pseudotransition states are sketched in Figure 7C,D, respectively.

The data of Table 2 indicate that for the model with 3-*tert*-butyl-substituted ligand **1**, for the (*R*,*R*) chirality of coordination of the ligand, the *si* (rather than the *re*) monomer coordination (and primary insertion) is favored. This is due to a larger steric hindrance of the

tert-butyl group with respect to the six-membered ring of the ligand, which makes the growing chain orientations with $\theta_1 \approx +60°$ energetically favored with respect to those with $\theta_1 \approx -60°$ (Figures 6B). This, in turn, favors the primary insertion of the *si* monomer (Figure 7A,C) with respect to the *re* monomer.[3] Hence, for the model complex with ligand **1** *tert*-butyl substituted in position 3, a comparison of the ΔE_{enant} and ΔE^*_{enant} values of Table 2 indicates a slightly reduced enantioselectivity but one that is in favor of the opposite monomer enantioface. It is worth noting that while the general prediction of enantioselectivity in favor of the *re* enantioface for metallocene complexes with π-ligand (*R*,*R*) coordinated[3a] has received several experimental supports,[26a,28,29] at the moment there is no experimental evidence of enantioselectivity in favor of the *si* enantioface for the metallocene complexes with 3-*tert*-butyl-substituted bis(indenyl) ligands (*R*,*R*) coordinated. Moreover, while the calculated enantioselectivity of occasional regioirregular insertion, in agreement with the available experimental data, is generally very large, for the particular case of the model based on 3-*tert*-butyl-substituted ligand **1** it is small ($E_d - E_e$ in Figure 6B). However, since for the corresponding catalytic system the amount of regioirregularities is below the limit of detectability, this prediction of poor enantioselectivity for regioirregular insertions cannot be easily verified.

As for the nonbonded energy contribution to the regiospecificity, the largest ΔE_{regio} and ΔE^*_{regio} values of Table 2 have been obtained for the model complex with ligand **1** *tert*-butyl substituted in position 3. In fact, in models suitable for secondary insertion, the methyl group of the *si*-coordinated propene is at short distances with respect to methyl groups of the *tert*-butyl substituent ($d_{C-C} \approx 3.4$ Å in Figure 7B,D) while the methyl group of the *re*-coordinated propene is at short distances with respect to C atoms of the six-membered ring of an indenyl ligand. On the contrary, for the case of models for primary insertion (Figure 7A,C), the distances of the methyl group of propene from the carbon atoms of the *tert*-butyl groups as well as of the six-membered rings are larger than 3.7 Å.

The reported calculations for the model with 3-*tert*-butyl-substituted ligand **1** are in qualitative agreement with observed behaviors of corresponding catalytic systems. In particular, the large ΔE_{regio} or ΔE^*_{regio} values well account for the substantial undetectability of regioirregular insertions.[11a]

4. Conclusions

Following our traditional molecular mechanics approach for catalytic model complexes, the nonbonded energy contribution to the regioselectivity, as well as the enantioselectivities for primary and secondary insertions, have been approximated by energy differences between minimum energy situations close to the transition states of the insertion reactions (preinsertion intermediates) or between pseudotransition states.

The calculated enantioselectivities and regioselectivities, for model complexes based on C_2-symmetric *ansa*-zirconocenes **1**−**3**, unsubstituted or alkyl substituted in different positions, have been collected in Table 2. As discussed in previous pages,[3,9] and in agreement with several experimental results,[26a,28,29] the models predict that the *re* and *si* monomer coordination (and primary insertion) is generally favored for the (*R*,*R*) and (*S*,*S*) chirality of coordination of the π-ligands, respectively. The present calculations on models with 3-methyl-substituted ligand **1** are able to account for the poor enantioselectivity of corresponding catalytic systems, while those relative to models with 3-*tert*-butyl-substituted ligand **1** predict a substantial enantioselectivity but in favor of the opposite monomer enantioface (*si* and *re* for (*R*,*R*)- and (*S*,*S*)-coordinated π-ligand, respectively).

As for the nonbonded energy contribution to the regiospecificity, nonbonded energy interactions are able to account for the increases and decreases of regiospecificity experimentally observed after methyl substitution in position 2 (for ligands **1** and **2**) and dimethyl substitutions in positions 4,7 (for ligands **1** and **3**), respectively. In particular, strong interactions of the methyl group of the coordinated propene occur with the 2-methyl substituent in models suitable for secondary insertion (Figure 3) while with the 4-methyl substituent in models suitable for primary insertion (Figure 4). For catalytic systems based on C_2-symmetric *ansa*-metallocenes, substantial increases of molecular masses of isotactic polypropylene samples have been observed as a consequence of 2-methyl substitutions of the bridged π-ligands.[10a,30] Experimental data relative to the monomer concentration dependence of the molecular masses[10b,31] as well as molecular mechanics calculations[32] indicate that the presence of 2-methyl substituents inhibits the chain termination by β-hydrogen transfer to the monomer.

The calculated nonbonded energy contribution to the regiospecificity for the model based on ligand **1** incrases substantially after 3-*tert*-butyl substitution. This is due to nonbonded interactions between the methyl group of the coordinated propene and methyl groups of the *tert*-butyl substituent, which are stronger in models suitable for secondary insertion than in models suitable for primary insertion (Figure 6). This accounts for the high regiospecificity of corresponding isospecific catalytic systems, which is comparable with those obsered for syndiospecific and aspecific *ansa*-zirconocene-based catalytic systems.

The high regiospecificity of catalytic systems based on ligand **1**, after 3-methyl substitution,[6n] is accounted for by their poor enantioselectivity.[11a]

Acknowledgment. Financial support of the "Ministero dell'Università e della Ricerca Scientifica e Tecnologica" and of the "Consiglio Nazionale delle Richerche" of Italy is gratefully acknowledged.

References and Notes

(1) (a) Schnutenhaus, H.; Brintzinger, H. H. *Angew. Chem., Int. Ed. Engl.* **1979**, *18*, 777. (b) Wild, F.; Zsolnai, L.; Huttner, G.; Brintzinger, H. H. *J. Organomet. Chem.* **1982**, *232*, 233. (c) Collins, S.; Kuntz, B.; Taylor, N.; Taylor, N.; Ward, D. *J. Organomet. Chem.* **1988**, *342*, 21. (d) Wild, F.; Wasiucionek, M.; Huttner, G.; Brintzinger, H. H. *J. Organomet. Chem.* **1985**, *288*, 63. (e) Schäfer, A.; Karl, E.; Zsolnai, L.; Huttner, G.; Brintzinger, H. H. *J. Organomet. Chem.* **1987**, *328*, 87. (f) Wiesenfeldt, H.; Reinmuth, A.; Barsties, E.; Evertz, K.; Brintzinger, H. H. *J. Organomet. Chem.* **1989**, *369*, 359. (g) Burger, P.; Hortmann, K.; Diebold, J.; Brintzinger, H. H. *J. Organomet. Chem.* **1991**, *417*, 9. (h) Brintzinger, H. H. In *Transition Metals and Organometallics as Catalysts for Olefin Polymerization*; Kaminsky, W., Sinn, H., Eds.; Springer-Verlag: Berlin, 1988; p 249.

(2) (a) Ewen, J. *J. Am. Chem. Soc.* **1984**, *106*, 6355. (b) Ewen, J. US Patent 4,522,982 to Exxon, 1985. (c) Ewen, J. In *Catalytic Polymerization of Olefins, Studies in Surface Science and Catalysis*; Keii, T., Soga, K., Eds.; Elsevier: New York, 1986; Vol. 25, p 271. (d) Ewen, J.; Haspeslagh, L.; Atwood, J.;

Zhang, H. *J. Am. Chem. Soc.* **1987**, *109*, 6544. (e) Ewen, J.; Haspeslagh, L.; Elder, M.; Atwood, J.; Zhang, H.; Cheng, H. In *Transition Metals and Organometallics as Catalysts for Olefin Polymerization*; Kaminsky, W., Sinn, H., Eds.; Springer-Verlag: Berlin, 1988; p 281. (f) Kaminsky, W.; Külper, K.; Brintzinger, H. H.; Wild, F. *Angew. Chem., Int. Ed. Engl.* **1985**, *24*, 507. (g) Kaminsky, W.; Külper, K.; Buschermöhle, M.; Lüker, H. US Patent 4,769,510 to Hoechst, 1988. (h) Kaminsky, W. *Angew. Makromol. Chem.* **1986**, *145/146*, 149. (i) Kaminsky, W. In *Catalytic Polymerization of Olefins*; Keii, T., Soga, K., Eds.; Elsevier: New York, 1986; p 293.

(3) (a) Corradini, P.; Guerra, G.; Vacatello, M.; Villani, V. *Gazz. Chim. Ital.* **1988**, *118*, 173. (b) Cavallo, L.; Guerra, G.; Oliva, L.; Vacatello, M.; Corradini, P. *Polym. Commun.* **1989**, *30*, 16. (c) Cavallo, L.; Corradini, P.; Guerra, G.; Vacatello, M. *Polymer* **1991**, *32*, 1329. (d) Cavallo, L.; Guerra, G.; Vacatello, M.; Corradini, P. Chirality **1991**, *3*, 299. (e) Guerra, G.; Cavallo, L.; Moscardi, G.; Vacatello, M.; Corradini, P. *J. Am. Chem. Soc.* **1994**, *116*, 2988. (f) Guerra, G.; Cavallo, L.; Moscardi, G.; Vacatello, M.; Corradini, P. *Macromolecules* **1996**, *29*, 4834.

(4) (a) Castonguay, L.; Rappé, A. *J. Am. Chem. Soc.* **1992**, *114*, 5832. (b) Hart, J.; Rappé, A. *J. Am. Chem. Soc.* **1993**, *115*, 6159. (c) Kawamura-Kuribayashi, H.; Koga, N.; Morokuma, K. *J. Am. Chem. Soc.* **1992**, *114*, 8687. (d) Van der Leek, Y.; Angermund, K. Refke, M.; Kleinschmidt, R.; Goretzki, R.; Fink, G. *Chem. Eur. J.* **1997**, *3*, 385.

(5) (a) Zambelli, A.; Ammendola, P.; Grassi, A.; Longo, P.; Proto, A. *Macromolecules* **1986**, *19*, 2703. (b) Longo, P.; Grassi, A.; Pellecchia, C.; Zambelli, A. *Macromolecules* **1987**, *20*, 1015.

(6) (a) Soga, K.; Shiono, T.; Takemura, S.; Kaminsky, W. *Makromol. Chem., Rapid Commun.* **1987**, *8*, 305. (b) Grassi, A.; Zambelli, A.; Resconi, L.; Albizzati, E.; Mazzocchi, R. *Macromolecules* **1988**, *21*, 617. (c) Cheng, H.; Ewen, J. *Makromol. Chem.* **1989**, 1931. (d) Tsutsui, T.; Ishimaru, N.; Mizuno, A.; Toyota, A.; Kashiwa, N. *Polymer* **1989**, *30*, 1350. (e) Tsutsui, T.; Mizuno, A.; Kashiwa, N. *Makromol. Chem.* **1989**, *190*, 1177. (f) Tsutsui, T.; Kioka, M.; Toyota, A.; Kashiwa, N. In *Catalytic Olefin Polymerization, Studies in Surface Science and Catalysis*; Keii, T., Soga, K., Eds.; Elsevier: New York, 1990; Vol. 56, p 493. (g) Rieger, B.; Chien, J. *Polym. Bull.* **1989**, *21*, 159. (h) Rieger, B.; Mu, X.; Mallin, D.; Rausch, M.; Chien, J. *Macromolecules* **1990**, *23*, 3559. (i) Chien, J.; Sugimoto, R. *J. Polym. Sci., Part A: Polym. Chem.* **1991**, *29*, 459. (j) Mizuno, A.; Tsutsui, T.; Kashiwa, N. *Polymer* **1992**, *33*, 254. (k) Busico, V.; Cipullo, R. *J. Organomet. Chem.* **1995**, *497*, 113. (l) Spaleck, W.; Antberg, M.; Aulbach, M.; Bachmann, B.; Dolle, V.; Haftka, S.; Küber, F.; Rohrmann, J.; Winter, A. In *Ziegler Catalysts*; Fink, G., Mülhaupt, R.; Brintzinger, H. H., Eds.; Springer-Verlag: Berlin, 1995; p 83. (m) Resconi, L.; Fait, A.; Piemontesi, F.; Colonnesi, M.; Rychlicki, H.; Zeigler, R. *Macromolecules* **1995**, *28*, 6667. (n) Resconi, L.; Piemontesi, F.; Camurati, I.; Rychlicki, H.; Colonnesi, M.; Balboni, D. *Polym. Mater. Sci. Eng.* **1995**, *73*, 516.

(7) (a) Ewen, J.; Elder, M. J.; Jones, R. L.; Curtis, S.; Cheng, H. N. In *Catalytic Olefin Polymerization, Studies in Surface Science and Catalysis*; Keii, T., Soga, K., Eds.; Elsevier: New York, 1990; Vol. 56, p 439. (b) Herfert, N.; Fink, G. *Makromol. Chem.* **1992**, *193*, 773.

(8) (a) Resconi, L.; Piemontesi, F.; Franciscono, G.; Abis, L.; Fiorani, T. *J. Am. Chem. Soc.* **1992**, *114*, 1025. (b) Lee, I. M.; Gauthier, W. J.; Ball, J. M.; Iyengar, B.; Collins, S. *Organometallics* **1992**, *11*, 2115.

(9) Guerra, G.; Longo, P.; Cavallo, L.; Corradini, P.; Resconi, L. *J. Am. Chem. Soc.* **1997**, *119*, 4394.

(10) (a) Röll, W.; Brintzinger, H. H.; Rieger, B.; Zolk, R. *Angew. Chem., Int. Ed. Engl.* **1990**, *29*, 279. (b) Stehling, V.; Diebold, J.; Kirsten, R.; Röll, W.; Brintzinger, H. H. *Organometallics* **1994**, *13*, 964.

(11) (a) Ewen, J.; Longo, P. Private communication. (b) Resconi, L.; Piemontesi, F.; Nifant'ev, I. E.; Ivichenko, P. V. PCT WO96 22,995 to Montell.

(12) Resconi, L.; Piemontesi, F.; Camurati, I.; Balboni, D.; Sironi, A.; Moret, M.; Rychlicki, H.; Zeigler, R. *Organometallics* **1996**, *15*, 5046.

(13) Resconi, L.; Moscardi, G. *Polym. Prepr. (Am. Chem. Soc., Dis. Polym. Chem.)* **1997**, *38*, 832.

(14) Hanson, K. R. *J. Am. Chem. Soc.* **1966**, *88*, 2731.

(15) (a) Cahn, R. S.; Ingold, C.; Prelog, V. *Angew. Chem., Int. Ed. Engl.* **1966**, *5*, 385. (b) Prelog, V.; Helmchem, G. *Angew. Chem., Int. Ed. Engl.* **1982**, *21*, 567.

(16) Schlögl, K. *Top. Stereochem.* **1966**, *1*, 39.

(17) (a) Cossee, P. *Tetrahedron Lett.* **1960**, *17*, 12. (b) *Ibid.* **1960**, *17*, 17. (c) Cossee, P. *J. Catal.* **1964**, *3*, 80. (d) Hine, J. *J. Org. Chem.* **1966**, *31*, 1236. (e) Hine, J. *Adv. Phys. Org. Chem.* **1977**, *15*, 1. (f) Venditto, V.; Guerra, G.; Corradini, P.; Fusco, R. *Polymer* **1990**, *31*, 530. (g) Venditto, V.; Guerra, G.; Corradini, P.; Fusco, R. *Eur. Polym. J.* **1991**, *27*, 45.

(18) (a) Kraudelat, H.; Brintzinger, H. H. *Angew. Chem., Int. Ed. Engl.* **1990**, *29*, 1412. (b) Brintzinger, H. H.; Fischer, D.; Mülhaupt, R.; Rieger, B.; Waymouth, R. M. *Angew. Chem., Int. Ed. Engl.* **1995**, *34*, 1143. (c) Piers, W. E.; Bercaw, J. E. *J. Am. Chem. Soc.* **1990**, *112*, 9406. (d) Clawson, L.; Soto, J.; Buchwald, S. L.; Steigerwald, M. L.; Grubbs, R. H. *J. Am. Chem. Soc.* **1985**, *107*, 3377.

(19) Woo, T. K.; Fan, L.; Ziegler, T. *Organometallics* **1994**, *13*, 432.

(20) (a) Corradini, P.; Barone, V.; Fusco, R.; Guerra, G. *Eur. Polym. J.* **1979**, *15*, 133. (b) Corradini, P.; Barone, V.; Fusco, R.; Guerra, G. *Gazz. Chim. Ital.* **1983**, *113*, 601.

(21) Doman, T. N.; Hollis, T. K.; Bosnich, B. *J. Am. Chem. Soc.* **1995**, *117*, 1352.

(22) Brooks, B. R.; Bruccoleri, R. E.; Olafson, B. D.; States, D. J.; Swaminathan, S.; Karplus, M. *J. Comput. Chem.* **1983**, *4*, 187.

(23) Resconi, L.; Jones, R.; Rheingold, A.; Yap, G. *Organometallics* **1996**, *15*, 998.

(24) With reference to Figure 10C of ref 9, $E_e - E_a$ gives a rough approximation of the nonbonded energy contribution to: $\Delta\Delta E^{\ddagger}_{reg}$(isospecific) $\approx \Delta E^{\ddagger}_{s,w} - \Delta E^{\ddagger}_{coord,r}$.

(25) Rieger, B.; Reinmuth, A.; Röll, W.; Brintzinger, H. H. *J. Mol. Catal.* **1993**, *82*, 67.

(26) (a) Ewen, J.; Elder, M. J.; Jones, R. L.; Hasplslagh, L.; Atwood, J. L.; Bott, S. G.; Robinson, K. *Makromol. Chem. Macromol. Symp.* **1991**, *48/49*, 253. (b) Ewen, J.; Haspeslagh, L.; Elder, M. J.; Atwood, J. L.; Zhang, H.; Cheng, N. In *Transition Metals and organometallics as Catalysis for Olefin Polymerization*; Kaminsky, W., Sinn, H., Eds.; Springer: Berlin, 1988; p 281.

(27) With reference to Figure 10A of ref 9, $\Delta\Delta E^{\ddagger}_{reg}$(aspecific) $\approx \Delta E^{\ddagger}_{s} - \Delta E^{\ddagger}_{p}$, where $\Delta E^{\ddagger}_{s} \ll \Delta E^{\ddagger}_{p}$.

(28) Pino, P.; Cioni, P.; Wei, J. *J. Am. Chem. Soc.* **1987**, *109*, 6189.

(29) Herzog, T. A.; Zubris, O. L.; Bercaw, J. E. *J. Am. Chem. Soc.* **1996**, *118*, 11988.

(30) (a) Mise, T.; Miya, S.; Yamazaki, H. *Chem. Lett. (Japan)* **1989**, 1853. (b) Spaleck, W.; Kuber, F.; Winter, A.; Rohrmann, J.; Bachmann, B.; Antberg, M.; Dolle, V.; Paulus, E. F. *Organometallics* **1994**, *13*, 954.

(31) Jüngling, J.; Mühlhaupt, R.; Stehling, U.; Brintzinger, H. H.; Fisher, D.; Langhauser, T. *J. Polym. Sci., Polym. Chem.* **1995**, *33*, 1305.

(32) Cavallo, L.; Guerra, G. *Macromolecules* **1996**, *29*, 2729.

MA980238W